AVS Quantum Science

The Penrose process in nonlinear optics

Cite as: AVS Quantum Sci. 4, 010501 (2022); https://doi.org/10.1116/5.0073218
Submitted: 28 September 2021 • Accepted: 18 January 2022 • Published Online: 09 February 2022

Maria Chiara Braidotti, Francesco Marino, Ewan M. Wright, et al.

AVS Quantum Science PERSPECTIVE scitation.org/journal/aqs

The Penrose process in nonlinear optics

Cite as: AVS Quantum Sci. 4, 010501 (2022); doi: 10.1116/5.0073218
Submitted: 28 September 2021 · Accepted: 18 January 2022 ·
Published Online: 9 February 2022

Maria Chiara Braidotti,[1] Francesco Marino,[2,3] Ewan M. Wright,[4,5] and Daniele Faccio[1,4]

AFFILIATIONS

[1]School of Physics and Astronomy, University of Glasgow, G12 8QQ Glasgow, United Kingdom
[2]CNR-Istituto Nazionale di Ottica, L.go E. Fermi 6, I-50125 Firenze, Italy
[3]INFN, Sez. di Firenze, Via Sansone 1, I-50019 Sesto Fiorentino (FI), Italy
[4]Wyant College of Optical Sciences, University of Arizona, Tucson, Arizona 85721, USA
[5]Institute of Photonics and Quantum Sciences, Heriot-Watt University, EH14 4AS Edinburgh, United Kingdom

ABSTRACT

Penrose process is a mechanism by which energy may be extracted from the rotation of a Kerr black hole. The goal of this Perspective is to describe the elements that combine to allow a tabletop nonlinear optics experiment involving laser propagation in a medium to provide a versatile platform for elucidating the intimate details of the Penrose process. Key elements include propagation in a thermo-optic medium viewed as a photon fluid, rotating black hole geometries in a photon superfluid, and the Zel'dovich effect, and we highlight connections to the work of Roger Penrose throughout. In addition, we point out how the Penrose process has led to the notion of geometry-induced phase-matching in nonlinear optics, thereby highlighting the synergy between the fields of nonlinear optics and analog black holes.

I. INTRODUCTION

It is a great pleasure for us all to participate in this celebration of the magnificent career of Sir Roger Penrose culminating in him being awarded the 2020 Nobel Prize in Physics. His seminal works in the fields of general relativity, black hole physics, and quantum theory have been a continuing source of inspiration for us.[1,2] In particular, several years ago we embarked on a research program to find an analog-gravity system that would allow for the experimental exploration of the physics involved in the Penrose process. Our research program, both theory and experiment, has come to fruition during 2021 and it is the goal of this Perspective to describe the physics involved that allows nonlinear optics to provide a versatile platform for the exploration of the Penrose process.[3–11]

In a seminal paper published in 1969, Roger Penrose put forward his marvelous discovery that a rotating black hole can store rotational energy in the circulating spacetime surrounding its ergoregion.[1] Since the ergoregion is located outside of the event horizon, this rotational energy can therefore in principle be extracted, with concomitant decrease in the black hole's rotation rate. In particular, a particle of a given initial energy impinging on the ergoregion of the black hole may subsequently split into two parts. Then, if one part becomes trapped within the ergoregion and thereby acquires a negative energy, the other part can attain an energy larger than the initial value if it escapes from the black hole: This is the Penrose process. For the case of waves, this is often referred to as Penrose superradiance, a term coined by Misner, as an incident wave can be amplified upon reflection from the black hole.[12] The very first experimental demonstration of Penrose superradiance was performed in a hydrodynamic setting using rotating vortices in a water tank.[13]

This work inserts itself in a broader field called analog gravity, born in 1981 when Bill Unruh showed that analog Hawking radiation was present near wave horizons in a hydrodynamical fluid flow.[14] Since then, many different analogs of inaccessible gravitational phenomena have been proposed through tabletop experiments: examples include Hawking radiation, boson stars, and superradiance, which have been studied in different physical systems as nonlinear optics and Bose–Einstein condensates to hydrodynamics.[8,10,15–23] Studies on superradiance, in particular, have also been proposed in superfluids, as in Refs. 5–7 and 24, though the first experimental proof of this Penrose amplification in optical superfluids has been recently provided by us.[25] Superfluids have proved to be a versatile platform also for other gravitational phenomena such as Hawking radiation, optical analogs of the event horizon, and analog black holes.[11,26–33]

Our goal in this Perspective is to overview key physical ideas that have allowed us to explore the fine details of the Penrose process using a relatively modest nonlinear optics experiment involving the propagation of a laser beam in a thermo-optic medium. For this purpose, we shall highlight the key physics from four of our works in the following

sections, details being available in the original papers.[4,5,11,25] To provide the reader a birds eye view of the paper, we first provide a road map to the topics that will be addressed in the following sections. Section II provides a description of the paraxial wave equation for beam propagation in a nonlinear thermo-optic medium and the relation of this to the Schrödinger–Newton equation. The thermo-optic light–matter interaction is an example of a third-order optical nonlinearity in which two photons from a strong pump beam can mix with an incident signal photon to create a fourth distinct idler photon. This four-wave mixing (FWM) process is the means by which an incident particle can be induced to split into two parts as needed for the Penrose process. We then describe how the thermo-optic system can be viewed as a photon fluid, complete with the notion of Bogoliubov excitations with respect to the strong pump beam. The power of this approach is that it is these Bogoliubov excitations that best serve as the quasi-particles that participate in the Penrose process. Building on the photon fluid view, in Sec. III we describe how rotating two-dimensional black hole geometries can be realized by considering vortex pump beams that carry orbital angular momentum (OAM). These photon superfluids have both ergospheres and horizons and can serve as analog black holes for the Penrose process. Finally, in Sec. IV we bring all these ideas together and describe a geometry in which the Penrose process can be explored in detail in our analog system, including amplified reflection, the generation of negative norm modes, and the relation of this to the so-called Zel'dovich–Misner condition.[12,34] We also highlight how our study of the Penrose process has in turn led to the notion of geometry-induced phase-matching in nonlinear optics.[4] Our summary and outlook is given in Sec. V.

II. NONLINEAR OPTICS AND PHOTON FLUIDS

This section describes our analog system for realizing the Penrose process, first from a nonlinear optics perspective, and then from a photon fluid perspective. Both perspectives are important, nonlinear optics for understanding the experiment, and the photon fluid view for interpreting the results.

A. Thermo-optic propagation

Our analog system involves the propagation of a monochromatic laser beam of wavelength λ in a thermo-optic medium. The evolution of the complex field envelope E is then governed in the paraxial approximation by the Nonlinear Schrödinger Equation (NSE)[35]

$$i\frac{\partial E}{\partial z}+\frac{1}{2k}\nabla_\perp^2 E+\frac{k}{n_0}\Delta n(|E|^2)E=0. \tag{1}$$

Here, the laser beam is taken to be propagating dominantly along the z axis, n_0 is the linear refractive index, $k=2\pi n_0/\lambda=n_0k_0$ is the wavenumber, and $\nabla_\perp^2$ is the transverse Laplacian describing beam diffraction. We note that the real vector electric field is related to the field envelope via

$$\mathbf{E}(\mathbf{r},z,t)=\frac{1}{2}\left[\mathbf{e}E(\mathbf{r},z)e^{ik(z-ct/n_0)}+c.c.\right], \tag{2}$$

where $\mathbf{r}=(x,y)$ is the transverse position vector and $\mathbf{e}$ the unit polarization vector. When using the scalar field approximation, it is therefore understood that the rapidly varying carrier wave $e^{ik(z-ct/n_0)}$ has been removed, and that all wavevectors derived from the field envelope E must be referenced with respect to the carrier value k.

In general, the nonlinear change in refractive index Δn in steady-state may be expressed as

$$\Delta n(\mathbf{r},z)=n_2\int R(\mathbf{r}-\mathbf{r}')|E(\mathbf{r}',z)|^2d\mathbf{r}'. \tag{3}$$

Physically, the propagating laser beam in our experiments is weakly absorbed by the medium leading to a temperature change, and in a thermo-optic medium this leads to a change in the refractive index of the medium that is proportional to the temperature change. The response function $R(\mathbf{r}-\mathbf{r}')$ in Eq. (3) accounts for the nonlocal thermal diffusion arising from the heat equation plus boundary conditions due to the finite size of the medium, the laser intensity $|E(\mathbf{r}',z)|^2$ being the source for the heating.[9,11] We remark that the NSE (1) in conjunction with the refractive-index change in Eq. (3) is related to the Schrödinger–Newton equation that is having wide application in the fields of boson stars, dark matter, and dark energy.[9,36] Penrose and Diosi have both pioneered the Schrödinger–Newton equation as a model for the collapse of a wave function due to the effects of gravity.[37–39]

For the experiments discussed here, the particular thermo-optic medium is composed of a solution of methanol and a low concentration of graphene nanoflakes (23×10^{-6} g/cm^3), providing a weak absorption of the pump input beam to enhance the thermo-optic effect with nonlinear coefficient $n_2<0$, that is a defocusing nonlinearity. More specifically, the nonlocal response may be written as $R(\mathbf{r})=\frac{1}{2\pi\sigma^2}K_0\left(\frac{|\mathbf{r}|}{\sigma}\right)$, where $K_0(s)$ is the zeroth-order modified Bessel function of the second kind, with σ being a measure of the transverse diffusion in the system.[9,11] Moreover, experiments with time gated measurements, performed over short times ($\sim$0.2 s in our case), have verified that a strong nonlinearity with a weak nonlocality ($\sigma\sim200$ μm) can be realized before thermal diffusion has reached the steady-state (around 20 s in our case).[11] In this case, as long as the beams involved have dimensions larger than σ, the nonlinearity is to a high-degree local with $\Delta n(\mathbf{r},z)=n_2|E(\mathbf{r},z)|^2$. A variety of experiments have been performed in both the highly nonlocal and quasi-local limits, and in the remainder of this paper we shall discuss both limits, making sure to distinguish them.

B. Nonlinear four-wave mixing

A fundamental process in third-order nonlinear optics, of which thermo-optics is an example, is four-wave mixing (FWM) in which three fields combine to produce a fourth wave.[35] To illustrate this, consider a strong pump beam solution of Eq. (1) that propagates unchanged along the z axis, $E(\mathbf{r},z)=\mathscr{E}_0(x,y)e^{i\beta z}$, with β the nonlinear change in the wavevector of the pump beam. Then, if a weak signal beam E_s is added to the pump beam a new weak beam E_i, termed the idler beam, will be generated by the nonlinearity, giving the total field

$$\begin{aligned}E(\mathbf{r},z)&=E_0(\mathbf{r},z)+E_s(\mathbf{r},z)+E_i(\mathbf{r},z)\\&=[\mathscr{E}_0(\mathbf{r},z)+\mathscr{E}_s(\mathbf{r},z)+\mathscr{E}_i(\mathbf{r},z)]e^{i\beta z},\end{aligned} \tag{4}$$

where it is assumed that the pump, signal, and idler can be distinguished, e.g., they are propagating at slightly different angles or have different optical angular momentum (OAM). By substituting the

expansion in Eq. (4) into the NSE (1) for a local nonlinearity, and linearizing in the weak signal and idler fields, we obtain[4]

$$\begin{aligned}\frac{\partial \mathscr{E}_s}{\partial z} &= \frac{i}{2k}\nabla_T^2 \mathscr{E}_s + ik_0 n_2\left[2|\mathscr{E}_0|^2\mathscr{E}_s + \mathscr{E}_0^2\mathscr{E}_i^*\right] - i\beta\mathscr{E}_s,\\ \frac{\partial \mathscr{E}_i}{\partial z} &= \frac{i}{2k}\nabla_T^2 \mathscr{E}_i + ik_0 n_2\left[2|\mathscr{E}_0|^2\mathscr{E}_i + \mathscr{E}_0^2\mathscr{E}_s^*\right] - i\beta\mathscr{E}_i.\end{aligned} \tag{5}$$

Here, the first term on the right-hand side of each equation describes beam diffraction, the second describes cross-phase modulation (XPM) from the pump, and the third term describes the FWM process in which the complex conjugate of the idler field acts as a source for the signal field and vice versa. Thus, if a strong pump and weak signal are injected together, then FWM will generate a weak idler, the basic physical process at work being that two pump photons combine with one signal photon to create an idler photon. Furthermore, the FWM process can produce amplification of the signal and idler fields, the required power coming from the pump, if phase-matching is satisfied, which requires that the interaction between the signal and idler is phase synchronized. The phase-matching conditions depend sensitively on both the XPM term in Eq. (5), the third term, and also the fourth term.[4]

C. Photon fluid picture

The formal similarity of the NSE (1) to the Gross–Pitaevskii equation that governs superfluid systems such as ultracold atomic gases has been recognized for some time.[26,29,30,40] This similarity is enhanced by introducing the time variable $\tau = n_0 z/c$, and it becomes clear that thermo-optic propagation provides an analog of a two-dimensional superfluid, a photon fluid. Then, writing the complex field in terms of its amplitude and phase, i.e., $E(\mathbf{r},z) = E_{bg}(\mathbf{r},z) \times \exp\left(i\phi(\mathbf{r},z)\right)$, the NSE (1) can be expressed for a local nonlinearity as the following two equations:

$$\begin{aligned}&\frac{\partial \rho}{\partial \tau} + \nabla(\rho \mathbf{v}) = 0,\\ &\frac{\partial \psi}{\partial \tau} + \frac{1}{2}v^2 + \frac{c^2 n_2}{n_0^3}\rho - \frac{c^2}{2k^2 n_0^2}\frac{\nabla^2\sqrt{\rho}}{\sqrt{\rho}} = 0,\end{aligned} \tag{6}$$

which are formally identical to the density and phase equations for a two-dimensional superfluid, or photon fluid in the present case. Here, the optical background intensity $|E_{bg}|^2$ is identified as the photon fluid density ρ and the phase ϕ defines the fluid velocity via the relation $\mathbf{v} = (c/kn_0)\nabla\phi = \nabla\psi$. The last term in the velocity equation in (6) corresponds to the quantum pressure and is absent in a classical fluid description. In the context of optics, the quantum pressure is intimately related to beam diffraction.

To proceed, we next consider small amplitude perturbations $E = (E_{bg} + \varepsilon)$ on the background field E_{bg}, which can be described within the Bogoliubov theory as sound waves on top of the photon fluid. In the case of a spatially *homogeneous* photon fluid, where E_{bg} is independent of $\mathbf{r}$, a sound mode of wavevector $\mathbf{K}$ and amplitude $\alpha_{\mathbf{K}}$ takes the plane-wave form

$$\varepsilon = \alpha_{\mathbf{K}} u_{\mathbf{K}}\, \exp\left(-i\Omega\tau + i\mathbf{K}\cdot\mathbf{r}\right) + \alpha_{\mathbf{K}}^* v_{\mathbf{K}} \exp\left(i\Omega\tau - i\mathbf{K}\cdot\mathbf{r}\right), \tag{7}$$

where the angular frequency Ω satisfies the dispersion relation

$$(\Omega - \mathbf{v}\cdot\mathbf{K})^2 = \frac{c^2 n_2 |E_{bg}|^2}{n_0^3}K^2 + \frac{c^2}{4k^2 n_0^2}K^4, \tag{8}$$

with $\mathbf{v}$ the background flow velocity. Since this dispersion relation is quadratic, it yields two frequencies for each $\mathbf{K}$, and for each of these there is an associated Bogoliubov mode representing a sound wave. Using the terminology of hydrodynamics, we note that for low frequencies the dispersion of the sound modes has a phononic character $\Omega \propto K$, whereas for higher frequencies the second term dominates and the sound modes acquire a quadratic dispersion $\Omega \propto K^2$ characteristic of particles. The separation between these two regimes defines a characteristic length $\xi = \frac{1}{2}\sqrt{n_0|n_2|\,|E_{bg}|^2}$, usually called the *healing length* in the Bose–Einstein condensate (BEC) literature.[6,7,21,22] As a result, only long-wavelength sound modes with $\Lambda \gg \xi$ follow a sonic dispersion with a constant sound speed $c_s = \sqrt{c^2|n_2|\,|E_{bg}|^2/n_0^3}$. This is of particular relevance, since only a linear dispersion guarantees superfluid behavior.

It remains to translate these results back into the language of optics: First, $K = \sqrt{K_x^2 + K_y^2}$ is the magnitude of the transverse wavevector of the light field in the transverse plane, which plays the role of a phonon wavevector in the superfluid. Second, $\Omega = -(c/n_0)\Delta K_z$ for the photon fluid is related to the change ΔK_z in the wavevector along the propagation axis: This is consistent with the fact that in the paraxial approximation all wavevectors are referred to the optical value k. In this way, we can have the analog of temporal dynamics in a two-dimensional superfluid system using time-independent propagation in a thermo-optic medium.

Finally, within the nonlinear optics view we consider signal and idler fields and their cross interaction via the pump field. In contrast, in the photon fluid picture we consider the Bogoliubov modes that arise as sound waves on top of the pump wave. However, physics cannot depend on the choice of perspective and we can always consider the signal and idler as superpositions of the Bogoliubov modes. Indeed, for our experiment on the Penrose process we consider an incident signal mode comprised of Bogoliubov modes, and it is breaking apart of the two Bogoliubov mode components that allows us to realize the required splitting.

D. Experiments

The Bogoliubov dispersion has been successfully measured in experiments in nonlocal media.[11,32] In particular, We have previously performed experiments to characterize the Bogoliubov mode frequencies versus wavevector K for a photon fluid using our thermal medium. First, using a technique traditionally used in oceanography, we performed direct measurements of the single-particle part of the dispersion relation of the elementary excitations on top of the photon fluid to detect its global flow.[11] This clearly revealed the quadratic particle-like part of the spectrum, but lacked the resolution to see the all-important linear phonon-like part characteristic of the superfluid regime. Second, using a pump-and-probe setup, we investigated the collective nature of low-wavevector sound modes of the fluid.[32] For this, we employed a straightforward extension of the previous Bogoliubov theory to nonlocal media leading to a modified Bogoliubov dispersion of the form

$$(\Omega - \mathbf{vK})^2 = \frac{c^2 n_2 |E_{bg}|^2}{n_0^3}\hat{R}(K, n_0\Omega/c)K^2 + \frac{c^2}{4k^2 n_0^2}K^4, \quad (9)$$

where $\hat{R} = 1/(1 + K^2\sigma^2)$ is the Fourier transform of the response function R. Using this, we were able to examine how the nonlocal nature of optical nonlinearity significantly alters the Bogoliubov dispersion even for relatively small wavevectors, and verify that superfluid behavior can arise in our system. Related works, Refs. 33, 41, and 42, report the observation of Bogoliubov dispersion for a photon fluid formed using an atomic vapor with a local nonlinearity. The approach used in these experiments is more robust than the one previously described and allows for a more precise characterization of the Bogoliubov dispersion curve relying on a measurement of the group velocity instead of directly accessing the phase velocity of the phonon modes.[32]

In this section, we have shown how the Bogoliubov modes behave in a homogeneous flow. Next in Sec. III, we turn to how an inhomogeneous flow gives rise to an effective curved metric and show how our analog system can be used to realize black hole geometries by using pump beams that carry orbital angular momentum (OAM). Later, in Sec. IV we further build upon this to show how we have an analog system to study the Penrose process.

III. ROTATING SPACETIME GEOMETRIES

We now discuss the more general case of Bogoliubov mode propagation on top of an *inhomogeneous* photon fluid.

Generally speaking, any inhomogeneous, neutrally stable state of a spatially extended nonlinear system provides an effective curved spacetime on which its (linear) elementary excitations can propagate (see, e.g., Ref. 15 and references therein). A particularly relevant example for our discussion is that of sound waves in a flowing fluid. Their velocity relative to the laboratory frame becomes in general a local function of space and time coordinates (although the wave still travels at the speed of sound relative to the flowing fluid). The acoustic trajectories or, using the language of relativity, the "sound cones" delimiting the region of causally connected events are implicitly defined by the quadratic equation

$$-c_s^2 dt^2 + (d\mathbf{x} - \mathbf{v}dt)^2 = 0, \quad (10)$$

where $c_s = c_s(\mathbf{x}, t)$ and $\mathbf{v} = \mathbf{v}(\mathbf{x}, t)$. In the simple case of a constant c_s and $\mathbf{v} = \mathbf{v}(\mathbf{x})$, one can readily see that the spatially dependent flow will tip the sound cone of a given event. In any closed region of supersonic flow, the cones tip past the vertical, forming a trapped surface and an event horizon for sound.

This class of metrics, i.e., as in Eq. (10), can be uniquely determined by linearizing the fluid equations around the background state. The result is an equation of motion formally equivalent to the Klein–Gordon equation for a massless scalar field in a curved spacetime.[14,43] The geometry is specified by a Lorentzian metric tensor, the acoustic metric, the null geodesics of which are the trajectories defined by (10). As such, the phonon dynamics exhibits an effective Lorentz invariance with the local speed of sound playing the role of the speed of light. The coefficients of the acoustic metric only depend on the fluid density, which determines also the sound speed, and the flow velocity. Hence, by tailoring the properties of the flow it is possible to simulate gravitational spacetimes and related phenomena, such as, e.g., Hawking radiation, superradiance, and cosmological particle production.[10,15]

A. From Bogoliubov quasi-particles to Klein–Gordon fields

We now derive the evolution equations of Bogoliubov modes in an inhomogeneous photon fluid and establish a connection with massless scalar fields propagating in a $(2+1)$ curved spacetime. To this aim, we perturb the NSE (here, we consider a local Kerr nonlinearity $\Delta n = n_2|E|^2$) around a background solution $E_{bg} = \rho_0^{1/2} e^{i\phi_0}$, using a different ansatz from the one in Sec. II, i.e., $E = E_0(1 + \varepsilon + \cdots)$. After some algebra, we obtain the bosonic Bogoliubov–de Gennes equations[44]

$$\left(\partial_T - i\frac{c}{2kn_0}\partial_S\right)\varepsilon = -i\frac{\omega}{n_0}n_2\rho_0(\varepsilon + \varepsilon^*), \quad (11)$$

$$\left(\partial_T + i\frac{c}{2kn_0}\partial_S\right)\varepsilon^* = i\frac{\omega}{n_0}n_2\rho_0(\varepsilon + \varepsilon^*), \quad (12)$$

where we introduced the usual comoving derivative $\partial_T = \partial_\tau + \mathbf{v}_0 \cdot \nabla$, with the time coordinate $\tau = n_0 z/c$ and $\mathbf{v}_0 = (c/kn_0)\nabla\phi_0$, and the (second-order) spatial differential operator $\partial_S = \frac{1}{\rho_0}\nabla \cdot (\rho_0 \nabla\ )$. The coefficients of the linearized equations so obtained depend on the background field E_{bg} only through its density or the optical phase. In particular, the information on the flow velocity is encoded in the curved coordinate T (the time in the free-falling frame) and separated by that on the density. Such a separation will greatly simplify the derivation of a sound-wave equation in the appropriate conditions.

In the spatially homogeneous case, where both the background density ρ_0 and velocity $\mathbf{v_0}$ do not depend on the transverse coordinates, the plane-wave solutions of Eqs. (11) and (12) satisfy the Bogoliubov dispersion relation (8), which, in terms of the local speed of sound and the healing length, can be rewritten as

$$(\Omega_B - \mathbf{v_0} \cdot \mathbf{K})^2 = c_s^2 K^2\left(1 + \frac{K^2}{K_c}\right). \quad (13)$$

Equation (13) has now the form of a superluminally modified dispersion relation, appearing in some phenomenological approaches to quantum gravity.[45] In this context, the length ξ is the critical wavenumber $K_c = 2\pi/\xi$ associated with the high-energy breakdown of Lorentz invariance, generally expected to occur at the Planck scale. Low-energy modes with $K \ll K_c$ instead obey the relativistic dispersion relation for a massless particle propagating at the "invariant universal speed" c_s. This is the so-called hydrodynamic limit or sonic approximation, also related to the onset of superfluid behavior, as remarked in Sec. II.

If the flow is inhomogeneous, a formal equivalence between such modes and massless scalar fields in curved spacetime can be established by linearizing Eqs. (6) around a background state: $\rho = \rho_0 + \rho_1$, $\psi = \psi_0 + \psi_1$, with $\rho_1, \psi_1 \ll \rho_0, \psi_0$.[7] In the limit $K \ll K_c$, the terms arising from linearization of the quantum pressure are negligible and the dynamics is fully described by a single second-order equation for the linearized velocity-potential. This is identical to the Klein–Gordon equation for a massless scalar field

$$\Box\psi_1 \equiv \frac{1}{\sqrt{-g}}\partial_\mu\left(\sqrt{-g}\,g^{\mu\nu}\,\partial_\nu\,\psi_1\right), \quad (14)$$

propagating in a $(2+1)$-dimensional curved spacetime the geometry described by the acoustic metric $g_{\mu\nu}$, with inverse $g^{\mu\nu}$ and determinant g as follows:

$$g_{\mu\nu} = \left(\frac{\rho_0}{c_s}\right)^2 \begin{pmatrix} -(c_s^2 - v_0^2) & -\mathbf{v}_0^{\mathrm{T}} \\ -\mathbf{v}_0 & \mathbf{I} \end{pmatrix}, \tag{15}$$

where $\mathbf{I}$ is the two-dimensional identity matrix. This is also the standard approach in analog-gravity models based on Bose–Einstein condensates (BECs).[16]

Equivalently, we can derive the acoustic metric from the Bogoliubov–de Gennes equations (11) and (12), which allows us to directly relate the complex Bogoliubov excitations to massless Klein–Gordon fields. To this end, we apply the operator $\left(\partial_T + i\frac{c}{2kn_0}\partial_S\right)\left(\frac{1}{\rho_0}\right)$ to Eq. (11) and after some algebra we obtain

$$\left(\partial_T + i\frac{c}{2kn_0}\partial_S\right)\frac{1}{\rho_0}\left(\partial_T - i\frac{c}{2kn_0}\partial_S\right)\varepsilon = \frac{c_s^2}{\rho_0}\partial_S\varepsilon. \tag{16}$$

We observe that Eq. (16) has the form of a wave equation except for the second term inside each bracket. These extra factors make indeed the equation be fourth order in space derivatives. On the other hand, the gravitational analogy holds for wavenumbers $K \ll K_c$, for which the dispersion relation takes the relativistic form $g^{\mu\nu}K_\mu K_\nu = 0$ where $K_\mu = (\Omega_B/c_s, \mathbf{K})$ and the higher-order spatial derivatives in Eq. (16) can be neglected. We remark that this approximation is mathematically equivalent to take the diffractionless limit $k \to \infty$.[5] In the photon fluid picture, the wavevector k appears only in the coefficient of the quantum pressure; therefore, taking the diffractionless limit corresponds to neglecting this term.[7] The superfluid Eq. (6) thus reduces to the Navier–Stokes equations for a barotropic, irrotational, and inviscid fluid, in which the Lorentz symmetry associated with the phonon dynamics is not explicitly broken.[43]

Under this approximation, and using the fact that the background density ρ_0 satisfies the continuity equation [the first of Eq. (6)] with $\mathbf{v} = \mathbf{v}_0$, Eq. (16) can be rewritten as

$$\Box\varepsilon \equiv -(\partial_T + \nabla\cdot\mathbf{v_0})\partial_T\varepsilon + \nabla\cdot(c_s^2\nabla\varepsilon) = 0, \tag{17}$$

where $\Box$ is the d'Alambertian operator associated with the $(2+1)$-dimensional acoustic metric $g_{\mu\nu}$.

The complex fluctuations ε can be easily linked to the real density and phase perturbations through the relations $\rho_1 = \rho_0(\varepsilon + \varepsilon^*)$ and $\phi_1 = (i/2)(\varepsilon^* - \varepsilon)$. By means of these expressions and using the relation between the optical phase and velocity-potential of the flow, $\psi_1 = (c/kn_0)\phi_1$, one can split Eq. (17) into two decoupled wave equations given by

$$\Box\psi_1 = 0, \tag{18}$$

$$\Box\frac{\rho_1}{\rho_0} = 0. \tag{19}$$

Equation (18) is the usual massless Klein–Gordon equation (14) for the velocity-potential perturbations ψ_1 describing a sound wave[14,43] in inhomogeneous fluids. An equation of the same form (19) is satisfied also by the relative density fluctuations ρ_1/ρ_0.

B. Optical vortices and rotating spacetimes

In the following, we focus on stationary and axisymmetric rotating spacetimes suitable for the observation of Penrose superradiance. The line element $ds^2 \equiv g_{\mu\nu}dx^\mu dx^\nu$ of a generic acoustic metric (15) in polar coordinates is (up to the conformal factor ρ_0^2/c_s^2)

$$ds^2 \sim -(c_s^2 - v_0^2)d\tau^2 - 2v_r dr d\tau - 2v_\theta r d\theta d\tau + dr^2 + (rd\theta)^2,$$

where $v_0^2 = v_r^2 + v_\theta^2$, $v_r = \partial_r\psi_0$ and $v_\theta = (1/r)\partial_\theta\psi_0$. Metrics of this form allow for the realization of a variety of spacetime geometries of interest in general relativity. In any region, where the total fluid velocity exceeds the speed of sound, none of the observers can remain at rest relative to an inertial observer at infinity: they are forced to corotate with the flow due to the supersonic dragging of inertial frames. An analog phenomenology is found within the ergosphere surrounding any spinning black hole. If c_s^2 is everywhere positive (no regions of evanescent sound waves), an event horizon requires a nonzero radial velocity. An outer-trapped surface, and thus an acoustic black hole, forms where the normal component of the fluid velocity is supersonic and everywhere inward pointing. In $(2+1)$-dimensions, this translates into the simple condition $-v_r > c_s$. In such a region, a sound wave will be swept inward by the flow and be trapped inside the horizon, formed where $-v_r = c_s$. This acts as a boundary in spacetime, which causally disconnects the interior from the exterior. The sign of v_r is crucial: a closed curve on which $v_r = c_s$ corresponds indeed to a white-hole horizon.

An acoustic spacetime with an ergoregion and horizon can be realized by a draining vortex flow[15] that mimics the main features of a rotating black hole spacetime. Recently, experimental evidence of an ergoregion and horizon (either black or white hole) in a $(2+1)$-dimensional spacetime has been provided in a photon fluid with thermo-optical nonlinearities using a background beam with phase $\psi_0 = n\theta - 2\pi\sqrt{r/r_0}$, where r_0 is an experimental parameter controlling the radial phase dependence of the beam.[11] Outside the vortex core, the profile $\rho_0(r)$ asymptotes to a constant density and the flow is well approximated by $v_\theta = cn/(kn_0 r)$ and by $v_r = -c\pi/(kn_0\sqrt{r_0 r})$. An ergoregion can then be created by controlling the beam intensity such that the speed of sound c_s passes from faster to slower than the total flow. Moreover, an horizon forms where $|v_r| = c_s$.

The similarity of the associated metric with the Kerr geometry becomes clearer through the following transformation of the time and the azimuthal coordinates:[46]

$$d\tau \to d\tau + \frac{|v_r|}{(c_s^2 - v_r^2)}dr; \quad d\theta \to d\theta + \frac{|v_r|v_\theta}{r(c_s^2 - v_r^2)}dr,$$

defined in the exterior region $(r_h < r < \infty)$, where $r_h = \xi^2/r_0$ given by the condition $|v_r| = c_s$ is the event horizon. Defining $\Omega_H = \frac{n\xi}{\pi r_h^2}c_s$, the metric takes the form

$$ds^2 \sim -\left(1 - \frac{r_h}{r} - \frac{r_h^4\Omega_H^2}{r^2}\right)c_s^2 d\tau^2 + \left(1 - \frac{r_h}{r}\right)^{-1}dr^2 - 2r_h^2\Omega_H d\theta d\tau + (rd\theta)^2. \tag{20}$$

We now compare (20) with the with the equatorial slice of the Kerr geometry in Boyer–Lindquist coordinates.[47] The latter has two coordinate singularities, corresponding to an inner and an outer horizon, given by the positive roots of the quadratic equation $1/g_{rr} = 0$, viz., $r_{in,out} = 1 \pm \sqrt{1 - a^2}$, where a is the angular momentum of the black hole in natural units. The two horizons are separated for any

finite value of the rotation speed, except for the extremal one, $a = 1$. On the other hand, the component g_{rr} in (20) does not contain any dependence on the azimuthal flow and the quadratic equation $1/g_{rr} = 0$ yields only one positive root (i.e., a single horizon), as in the non-rotational case. The radius of the ergosphere is given by the vanishing of the temporal component $g_{\tau\tau}$, i.e., $r_e = \frac{r_h}{2}\left(1 + \sqrt{1 + 4r_h^2\Omega_H^2}\right)$, where Ω_H is the angular velocity at the horizon. The mixed term $g_{\tau\theta} = 2r_h^2\Omega_H$ is responsible of the frame dragging due to the rotating spacetime and disappears when there is no rotation ($\Omega_H = 0$). In this case, $r_e = r_h$ and the metric (20) corresponds to the Schwarzschild's solution (on the plane identified by a zero polar angle).

Among the various properties of the above metric, the most relevant for the present discussion is the existence of an ergoregion. As we shall see in the remainder of this section, sound-like quasi-particles in this region can have negative energies, which allows either to extract energy from the vacuum or to amplify waves in a classical scattering process.[6] This is the key ingredient for Penrose superradiance[2] (see Ref. 48 for a review). The role of a horizon in this context is more subtle and is essentially to act as a one-way membrane that separates positive and negative energy modes from recombining at infinity. An event horizon thus provides vacuum with an intrinsic dissipative mechanism[49] and acts as an absorbing boundary for in-going modes.[50] For rotating black holes, the horizon prevents the onset of instabilities, as the negative energy modes are rapidly dissipated and removed from the system.

In hydrodynamic systems, though, an event horizon is generally not required to observe superradiant amplification. This has been clarified for example in Ref. 5 and supported by the deep connection between the phenomenon of superradiance and so-called "over-reflection" in fluids (reflection with amplification at the interface between subsonic and supersonic flows), which does not need any horizon or absorbing boundary to occur.[51–54] The only necessary condition is the existence of a region supporting negative energy modes. In fluids, this is provided by the ergoregion surrounding vortex cores.

While in the framework of general relativity, asymptotically flat spacetimes having an ergosphere but no horizon are linearly unstable (ergosphere instability[55,56]) this is generally not the case in quantum fluids. In particular, our vortices are quasi-solitonic structures with a quantized circulation, the intensity (i.e., the fluid density and thus the sound speed) goes to zero at the vortex core and, moreover, the scattering modes are Bogoliubov excitations with a supersonic dispersion relation. All these features substantially change the stability properties of the system. In particular, single-charge vortices are stable (except in the presence of very particular background beams). Higher-charge vortices can exhibit a kind of ergoregion instability, although mitigated or even quenched by dispersive effects inherent to Bogoliubov waves and by the density depletion around the vortex core (see Ref. 57 for an exhaustive discussion on this topic). This is not the case of our system, which operates far from the instability regime. We will thus consider vortex flows with a purely azimuthal velocity profile that are typically more easily achievable in quantum fluid platforms.

In photon fluids, an appropriate background indeed naturally arises from the self-trapping of a phase singularity embedded in a broad optical beam with orbital angular momentum (OAM), due to the counterbalanced effects of self-defocusing and diffraction.[58] The resulting pattern is characterized by a dark core and a helical wave front, $E_0 = \rho_0^{1/2}(r)e^{i\psi_0}$, where $\rho_0(0) = 0$ and $\psi_0 = n\theta$ with the integer n being the topological charge of the vortex. The associated azimuthal fluid flow is thus $v_\theta = cn/(kn_0 r)$. An analytical expression for the corresponding metric does not exist. However, well outside the vortex core the background asymptotes to a homogeneous density and thus an homogeneous sound speed. The condition $v_\theta = c_s$ thus gives the radius of the ergoregion, i.e., $r_e = n\xi/\pi$ and the line element can be written as

$$ds^2 \sim -\left(1 - \frac{r_e^2}{r^2}\right)c_s^2 d\tau^2 + dr^2 - 2r_e^2\Omega d\theta d\tau + (rd\theta)^2, \tag{21}$$

where we define $\Omega \equiv v_\theta(r_e)/r_e = c_s/r_e$ as the rotational frequency at the ergo-radius relative to the laboratory frame. This is essentially the background geometry used to demonstrate Penrose superradiance in our system. The role of the event horizon in the proposed photon fluid system is provided by a trapping potential generated by the phase singularity at the center of the pump vortex. As seen from the outside, this potential acts as a horizon as any energy that is trapped is effectively lost. Furthermore, at the center of the pump core, the intensity goes to zero, providing an effective dissipation for the phonon modes that cease to exist [this is not encoded in the metric of Eq. (21), which holds for the outer region].

IV. THE PENROSE PROCESS

In this section, we describe a geometry to explore the Penrose process in a photon fluid. Let us start by summarizing how the Penrose process occurs with an eye to what is needed to test it in a nonlinear optics experiment.

As previously outlined, the Penrose process was introduced by Roger Penrose in 1969 for the scattering of particles from a rotating black hole.[1] He noted that a particle, co-rotating with the black hole and remaining trapped inside, can be seen by an observer at infinity, i.e., in a reference frame compatible with that of a Minkowskian observer far from the black hole, as having negative energy. This observation led him to the possibility of extracting energy from the black hole, by exploiting its rotational energy, and to the formulation of the so-called Penrose process: If a lump of matter splits into two sub-parts inside the ergoregion and one of them remains trapped inside, the other component can gain energy at the expense of the black hole rotational energy and momentum, hence escaping from the black hole with an energy higher than its initial one.

Shortly after in 1971, Zel'dovich proposed similar ideas in the context of wave amplification from a rotating metallic cylinder.[34] He showed that low frequency electromagnetic waves impinging radially on a rotating conducting cylinder can gain energy in the scattering process if the cylinder spins fast enough such that the Doppler frequency becomes negative. Linking the original Zel'dovich proposal with Penrose's previous works, it is possible to define the Zel'dovich–Misner condition for the "superradiance" process, i.e., the anomalous reflection from rotating black holes, as defined by Misner.[12] The Zel'dovich–Misner condition for amplification is

$$\omega - m\Omega < 0, \tag{22}$$

where ω is the wave's angular frequency, m its angular momentum, and Ω is the magnitude of the angular velocity of the rotating object. This suggests the role of negative frequencies in this kind of amplification phenomena.

In the remainder of this section, we focus our attention on Penrose superradiance for waves in a photon fluid, i.e., the amplification of positive energy modes in the interaction with a rotating medium and the trapping of negative energy modes within the ergoregion. We will see how the Zel'dovich–Misner condition naturally arises in nonlinear optics as the phase-matching condition for the signal and idler waves.[4] Three features are essential for this description: (i) the distinction of positive and negative energy modes and (ii) the definition of the interaction, i.e., of the reflection and transmission coefficients of the modes in the scattering with the ergoregion; and (iii) the definition of the phase-matching condition.

A. Linearized theory: Positive and negative energy modes

Let us start by defining the geometry needed for the interaction between the perturbation (signal and idler waves) and the nonlinear pump background that allows to observe Penrose superradiance. The underling FWM parametric interaction between the pump beam with the signal and idler field suggests that the idler will be proportional to the complex conjugate of the signal wave, so that the signal and idler should be Laguerre–Gauss (LG) beams with comparable intensity profiles and OAM n and q, respectively. The two beams are chosen to be coaxial and co-propagating. The signal beam is referred as the positive frequency mode while the idler wave acts as the negative energy one. In the Penrose process, however, the negative energy mode gets trapped in the ergosphere. Let us consider a nonlinear vortex pump solution of the form

$$\begin{aligned} E(r,\theta,z) &= \mathscr{E}_0(r)e^{i(\beta z+\ell\theta)} \\ &= \sqrt{I_\ell}\, u_\ell(r)e^{i(\beta z+\ell\theta)}, \end{aligned} \tag{23}$$

where I_ℓ is the background intensity of the vortex of OAM ℓ and $u_\ell(r)$ is the corresponding vortex profile whose core size is denoted by r_ℓ. The vortex profile, which we take as real without loss of generality, obeys the equation

$$\beta u_\ell = \frac{1}{2k}\nabla_\ell^2 u_\ell + k_0 n_2 I_\ell u_\ell^3, \tag{24}$$

where $u_\ell(r)\to 1$ for $r \gg r_\ell$, and we have defined $\nabla_p^2 = (\partial^2/\partial r^2) + (1/r)(\partial/\partial r) - (p^2/r^2)$. The signal and the idler are chosen to be co-propagating with the pump mode while being loosely focused onto the pump ergoregion. To proceed, we first look at the propagation of the signal wave, corresponding to the positive energy Bogoliubov mode.

1. Signal propagation

For this analysis, we assume that the signal is negligibly depleted by the nonlinear interaction. In this limit, we may neglect the effect of the idler on the signal propagation to lowest order. Equation (5) for the signal propagation becomes

$$\frac{\partial \mathscr{E}_s}{\partial z} \approx \frac{i}{2k}\nabla_n^2 \mathscr{E}_s + \underbrace{2i\beta u_\ell^2(r)\mathscr{E}_s - i\beta \mathscr{E}_s}. \tag{25}$$

If we initially neglect the under-braced term, this equation has LG beam solutions, and in our case the input signal is a focused LG beam with radial mode index $p=0$, winding number n, and focused spot size w_0: We write the normalized solution for this in the form $V_n(r,z)e^{-i(1+|n|)\phi_G(z)}$, where $V_n(r,z)$ is the normalized z-dependent LG mode profile and we have explicitly separated out the Gouy phase shift that occurs through the beam focus, with $\phi_G(z) = \tan^{-1}(z/z_0)$, the Rayleigh range being $z_0 = kw_0^2/2$. The underbraced terms describe extra phase-shifting terms, and assuming that the LG beam is not too tightly focused (this assumption is justified by the fact that we are dealing with a photon fluid and hence we want low K to be in the phononic regime) the solution including these terms may be approximated as

$$\mathscr{E}_s(r,z) \approx c_s V_n(r,z)e^{-i(1+|n|)\phi_G(z)}e^{2i\beta\Gamma_n(z)z - i\beta z}, \tag{26}$$

where

$$\Gamma_n(z) = \int_0^\infty 2\pi r dr\, |V_n(r,z)|^2 u_\ell^2(r) \tag{27}$$

describes the variation of the signal phase due to penetration of the LG mode into the pump vortex core. The key result is that the signal phase varies as follows:

$$\begin{aligned} \phi_s(z) &= (2\beta\Gamma_n(z) - \beta)z - (1+|n|)\phi_G(z) \\ &= \Delta K_s(z)z - (1+|n|)\phi_G(z). \end{aligned} \tag{28}$$

We can approximate

$$\Delta K_s(z) \approx \Delta K_s(0) = 2\beta\Gamma_n(0) - \beta, \tag{29}$$

since most of the nonlinear interaction occurs within a Rayleigh range around the beam focus at $z=0$. The overlap factor $\Gamma_n(0)$ is such that $0 \le \Gamma_n(0) \le 1$ and can be computed numerically.

From the signal wavevector, it is possible to calculate the signal frequency shift, showing that the signal corresponds to the positive frequency mode. To evaluate the frequency shift $\Delta\omega_s = -(c/n_0)\Delta K_s$ of the incident signal field, we should consider it as the beginning of the signal propagation, when the mode is far from the beam focus, which is at $z=0$. Well before the focus, $\Gamma_n(z) \simeq 1$, and $\Delta K_s \simeq \beta$ is negative, being the medium nonlinearity defocusing ($n_2 < 0$). Hence, far from the ergoregion, the corresponding incident signal frequency is positive ($\Delta\omega_s > 0$), as required by the Penrose process.

2. Idler propagation: Role of negative frequencies

The idler propagation equation in Eq. (5) can be rewritten as[4]

$$\frac{\partial \mathscr{E}_i}{\partial z} = \frac{i}{2k}\nabla_q^2 \mathscr{E}_i + \underbrace{i2\beta\left[u_\ell^2(r)-1\right]}_{\text{waveguide}}\mathscr{E}_i + i\beta\mathscr{E}_i + \underbrace{i\beta u_\ell^2(r)\mathscr{E}_s^*}_{\text{source}}. \tag{30}$$

The underbraced source term in the above equation describes how the idler wave, which is absent at the input, is driven by the signal beam via the parametric interaction. Since the nonlinear parameter β is negative, the underbraced term $2|\beta|[1-u_\ell^2(r)] = k_0\Delta n(r)$ defines a two-dimensional guiding refractive-index profile. That is, $u_\ell^2(r)$ zero being at the pump vortex center $r=0$ and unity for $r \gg r_\ell$ away from the vortex core, $\Delta n(r) = 2|\beta|$ is maximum at $r=0$ and goes to zero away from the core. The pump vortex therefore creates a cross-phase-modulation (XPM)-induced waveguide that is experienced by the idler wave [this also underpins the XPM-induced nonlinear phase shift $2\beta\Gamma_n(z)$ experienced by the signal in Eq. (26)].

The idler wave can be guided inside the wave-guiding potential created by the pump. The spectrum of guided idler waves with OAM q can be found by solving the wave equation combining beam diffraction and the XPM-induced refractive-index profile. Neglecting the source term for the time being, and for idler fields of the form

$$\mathscr{E}_i(r,z) = c_i U_{pq}(r) e^{i(\beta_\ell + \Lambda_{pq})z}, \tag{31}$$

with radial mode-index p and wavevector $\Delta K_i = \beta + \Lambda_q$, this leads to the equation for the modes ($p = 0, 1, 2, \ldots$)

$$\left(\frac{1}{2k}\nabla_q^2 + 2\beta\left[u_\ell^2(r) - 1\right]\right) U_{pq}(r) = \Lambda_{pq} U_{pq}(r). \tag{32}$$

This eigenproblem can be solved for the guided idler modes for a given pump vortex profile $u_\ell(r)$ and value of the nonlinear parameter β_ℓ: Note that it is possible that no guided idler modes exist in which case the Penrose process cannot occur. The eigenvalues Λ_{pq} are positive and decrease with increasing p, so, for the present purposes, the lowest radial mode $p = 0$ is the relevant one: We hereafter drop the radial mode index for simplicity in notation, and assume $U_q(r)$ and Λ_q exist and are known, at least numerically.

The modal solution $U_q(r)$ allows us to evaluate the ergosphere radius in a more systematic way: This mode has a single-ringed intensity profile and one can find the radius r_q of the peak intensity. Physically, any idler energy excited by this guided mode will effectively be confined or trapped within the radius r_q, so we identify r_q with a viable measure of the radius of the ergosphere. The approach $r_e = r_q$ agrees quite well with the previous approximation, particularly for larger q.

In order for the idler mode to be guided, the wavevector has to be positive. Therefore, the frequency shift $\Delta\omega_i = -(c/n_0)\Delta K_i$ of the excited idler field is negative ($\Delta\omega_i < 0$). The idler mode plays the role of the negative frequency mode in the Penrose picture.

B. Phase-matching and the Zel'dovich–Misner condition

We next turn to the phase-matching condition from a nonlinear optics perspective, and how this is related to the Zel'dovich–Meisner condition.

1. Phase-matching

We return to the idler propagation Eq. (30) and use the approximation to the signal field in Eq. (26). To deduce the condition for the incident signal field to be able to excite a guided idler mode, we substitute a guided idler field of the form

$$\mathscr{E}_i(r,z) = c_i(z) e^{i\Delta K_i z} U_q(r), \tag{33}$$

into Eq. (30) and project onto the idler guided wave to obtain

$$\frac{dc_i}{dz} = i c_s^* \beta F(z) e^{\underbrace{-i(2\Delta K z - (1+|n|)\phi_G(z))}}, \tag{34}$$

where

$$\Delta K = \left(\frac{\Delta K_s + \Delta K_i}{2}\right) \tag{35}$$

and

$$F(z) = \int_0^\infty 2\pi r dr\, V_n^*(r,z) u_\ell^2(r) U_q^*(r). \tag{36}$$

The underbraced phase factor contains the phase-matching condition, i.e., the condition in nonlinear optics such that the different waves participating in the parametric process are in phase and their interaction is guaranteed. Due to the presence of the Gouy phase-shift term and in the vicinity of the focus at $z = 0$, the phase factor is approximately $(2\Delta K z - (1 + |n|)z/z_0)$, so that $\Delta K > 0$ is required to have the possibility of phase-matching. More generally, similar phase factors as in Eq. (34) appear in the theory of harmonic generation using focused beams, and there it is found that for tight focusing a requirement for harmonic generation to be possible is $\Delta K > 0$.[35]

To recap, the condition for idler guided wave excitation to be possible is

$$\Delta K = \left(\frac{\Delta K_s + \Delta K_i}{2}\right) = \underbrace{(2\beta\Gamma_n(0) - \beta)}_{signal} + \underbrace{(\beta + \Lambda_q)}_{idler} > 0. \tag{37}$$

This condition can be used to determine whether the guided idler waves can be excited, with possible accompanying observation of the Penrose process. A stronger statement is that if $\Delta K < 0$ the Penrose process cannot arise.

2. Zel'dovich–Misner condition

If we convert the requirement $\Delta K > 0$ to a frequency shift, we get $\Delta\omega = -(c/n_0)\Delta K < 0$, where $\Delta\omega = (\Delta\omega_s + \Delta\omega_i/2)$ is the average of the frequency shifts of the signal and idler fields, with $\Delta\omega_{s,i} = -(c/n_0)\Delta K_{s,i}$. Then, writing the frequency shift as $\Delta\omega = (\omega - \omega_p) = (\omega - m\Omega)$, with $m = n - \ell$, the condition to see the Penrose process becomes

$$(\omega - m\Omega) < 0, \tag{38}$$

which has the same form as the Zel'dovich–Misner condition. Here, ω is the average of the (unshifted) frequencies of the signal and idler fields $\omega_{s,i} = (\Delta\omega_{s,i} + \omega_p)$, and is explicitly given by

$$\omega = -\frac{c}{n_0}(2\beta\Gamma_n(0) + \Lambda_q + \beta_\ell). \tag{39}$$

It is worth noting that a condition for Penrose superradiance to occur is that $m > 0$, i.e., $n > \ell$, so the signal OAM n has to be larger than the pump OAM ℓ. This illustrates that the condition for the Penrose process coincides with the Zel'dovich–Misner condition, which in turn coincides with the phase-matching condition. The fact that these conditions coincide highlights that the phase-matching condition has its origin in the induced black hole geometry that arises from using pump and signal beams that are vortices carrying OAM. For this reason, we call this type of phase-matching geometrically induced as it is dependent on the presence of an ergosphere.

Summarizing, in the usual picture of the Penrose process a positive frequency incident signal field is amplified upon reflection and excites a negative frequency idler field that is trapped within the ergoregion. The chosen geometry of the interaction guarantees the signs of the frequency shifts of the modes involved in the process, i.e., $\Delta\omega_s > 0$ far from the ergoregion and $\Delta\omega_i < 0$ inside it.

C. The Noether currents: reflection and transmission coefficients

In order to pinpoint and quantify the superradiance amplification, we need to define the reflection R and transmission T coefficients of the scattering of the perturbation composed signal and idler, i.e., positive and negative frequency modes, from the rotating body. If superradiance occurs, the reflection coefficient R will be larger than 1 such that the incoming positive mode has gained energy in the scattering process. It has been shown[5,29] that the coupled equations of propagation (5) for the signal and idler fields are invariant under the global $U(1)$ phase-shift transformation, i.e., $(E_s, E_i) \to (E_s, E_i)e^{i\lambda}$, with λ being any real number. The $U(1)$ symmetry can also be found in the action (see Ref. 5). Following the Noether theorem, to every symmetry in the action corresponds a conserved quantity. The $U(1)$ symmetry is associated with the conservation of the Noether charge, such that for the current J^μ it holds that $\partial_\mu J^\mu = 0$.

It is possible to show that integrating this conservation relation ($\partial_\mu J^\mu = 0$) over the finite radius of the interaction, corresponding to the ergoregion in our system, one obtains a measure of the reflection and transmission coefficients. The time component J^0 of the current J^μ associated with the symmetry is $J^0 = |E_s|^2 - |E_i|^2$, and the conserved charge is

$$N(z) = \int_0^\infty (|E_S|^2 - |E_I|^2) r dr = \text{const.} \tag{40}$$

This quantity in BECs is usually proportional to the energy of the eigenstate of the coupled equations by the relation $\mathbb{E} = \hbar\omega N(z)$, where ω is the mode frequency. It is worth noticing that this quantity is not positive-definite, hence the energy of the eigenstate can be negative. As shown before, the negative norm modes in our system correspond to the idler wave. From this definition (40), it is possible to also define the reflection R and transmission T coefficients for the scattering of the perturbation from the flow edge, that is

$$\begin{aligned} R(z) &= \int_{r_e}^\infty \left(|E_S|^2 - |E_I|^2\right) r dr, \\ T(z) &= \int_0^{r_e} \left(|E_S|^2 - |E_I|^2\right) r dr. \end{aligned} \tag{41}$$

For normalized fields $R + T = 1$, hence, a gain in the amplitude of the reflected mode causes a decrease in the transmission coefficient T, which becomes negative ($T < 0$), and an increase in the reflection coefficient such that $R > 1$. The value of the R and T coefficients is strongly related to the current J_0 distribution in the (x, y) plane. Hence, J_0 plays a central role for establishing the presence of superradiance: a negative current ($J_0 < 0$) is present inside the scattering region r_e (causing a negative T and hence $R > 1$), and a positive current ($J_0 > 0$) outside r_e.[5] This reflects Penrose's physics based on the presence of negative energy modes (idler beam) inside r_e. In order to have a negative current inside r_e along the propagation distance z, the idler wave has to be trapped inside the scattering region, while the signal is scattered outside. If there is no trapping of the idler, then the positive and negative modes can interfere and change the resulting energy outcome. In real black holes, the mechanism that governs the disappearance of the negative energy mode is given by the event horizon, while in our system it is regulated by the presence of the trapping potential due to the intensity modulation in the pump core and the presence of quantum pressure in the superfluid.

D. Numerical simulations of the Penrose Process

In Ref. 4, the authors reported numerical simulations testing the theoretical model just illustrated in order to verify the presence of Penrose effect in a photon fluid. They simulated the system of coupled Eq. (5) in a defocusing nonlinear medium. To simplify the basic physical concepts involved, the pump beam is assumed to not evolve, i.e., to be constant along z, not undergoing absorption and having local nonlinearity. This last assumption is ensured by a proper choice of the nonlocal length, $\sigma < 200$ m with a gating of 0.2 s.[11] By choosing the dimensions of the beams involved to be larger than σ, the nonlinearity is to a high degree local. In both the numerical and experimental results reported below, the pump beam dimensions are of the order $\approx$1 cm. The pump and signal core sizes are larger than 0.1 cm and, hence, the system can be considered to be quasi-local.

The vortex pump background chosen for the simulations is

$$E_0(r) = N_0 \tanh(r)^{|l|} e^{il\theta}, \tag{42}$$

where ℓ is the vortex charge we fix as $\ell = 1$ and N_0 is the normalization constant. Furthermore, the signal field is a Laguerre–Gauss beam with OAM n, which we write at the focus at $z = 0$ as

$$E_s(r, z = 0) = N_s \left(\frac{r}{w}\right)^{|n|} e^{-\frac{r^2}{w^2}} e^{in\theta}, \tag{43}$$

where N_s is the normalization constant. The idler beam is chosen to be initially zero, as it will be created by the nonlinear interaction between the pump E_0 and the signal E_S along the evolution.

Figure 1 shows the difference in the signal and idler intensity propagation when superradiance does not occur [Figs. 1(a)–1(d)], due to the fact that one of the conditions above is not satisfied, and when superradiance conditions are met and hence there is amplification [Figs. 1(e)–1(h)]. The dashed lines in Fig. 1 mark the location of the ergoregion.

In panels (a)–(d) of Fig. 1 the signal OAM is $n = -1$ and idler OAM $q = 2l - n = 3$ and hence superradiance conditions are not met, with $(n - \ell) > 0$ not satisfied. Panels (a)–(b) of Fig. 1 show the signal and idler field propagation along z, respectively. We see that the idler field is initially absent (the input beams are the pump and signal only, no idler) and it is created along the propagation direction [panel (b)], hence the ergoregion is empty at the beginning. Since superradiance conditions are not met, the ergoregion is asymptotically empty, i.e., along the propagation the idler does not get trapped inside the ergoregion and the current J_0 in panel (c) is always positive. As a consequence, also the reflection coefficient is $R < 1$ [see panel (d) of Fig. 1]. We note that at the focal point, the signal in panel (a) of Fig. 1 interacts with the ergoregion and penetrates into it. However, asymptotically it comes out and does not remain trapped inside. In Fig. 1 [panels (e)–(h)], it is shown where superradiance conditions are met. The signal and idler OAM are $n = 2$ and $q = 0$, respectively. After the signal has scattered with the ergoregion, the idler beam [panel (f) of Fig. 1] is trapped inside it and stays there for the duration of the propagation. This means that negative frequencies are trapped during the interaction, while positive frequencies are reflected (no signal inside the ergoregion) and amplified. It is meaningful to report the plot of

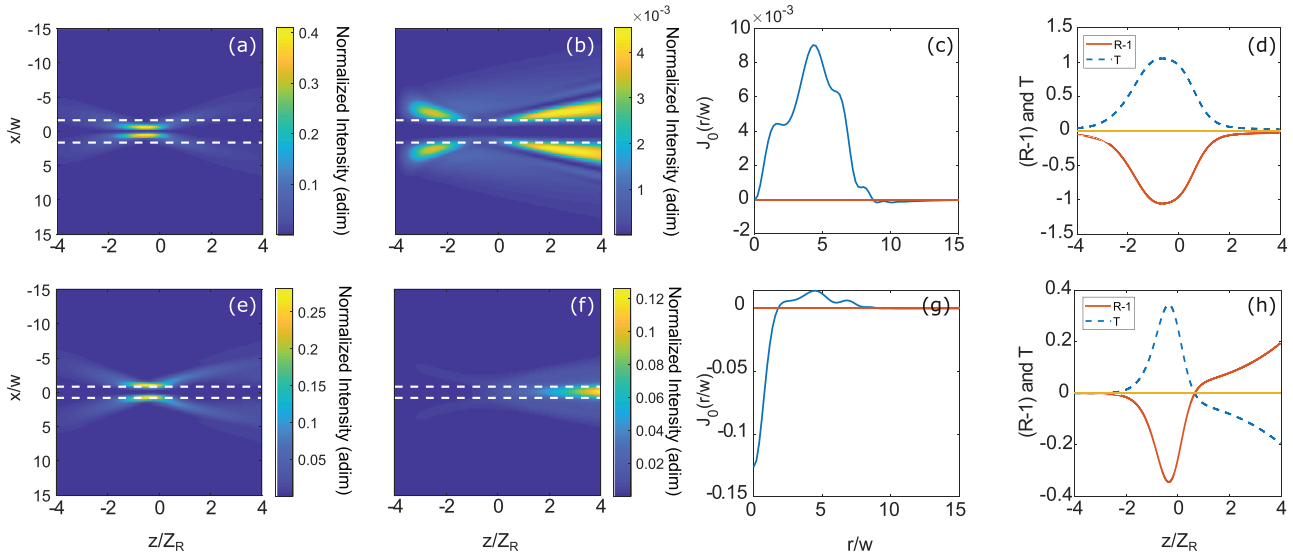

Fig. 1. The pump field E_0 has OAM $\ell = 1$. (a) and (b) Section at $y = 0$ of the simulated signal (a) and idler (b) intensity profiles along the propagation distance z/Z_R, computed using Eqs. (5). The input signal is a LG beam with OAM $n = -1$. The idler has OAM $q = 3$ and is not present at the input. No Penrose effect occurs in this case ($\Delta K < 0$). The dashed line marks the location of the ergoregion r_e. (c) Current $J_0(r/w)$ as a function of the normalized radius r/w. Red line shows the null current axis. (d) Reflection $R - 1$ and transmission T coefficients along the beams' evolution. (e)–(h) as in panel (a)–(d) for signal with OAM $n = 2$ and idler with OAM $q = 0$, such that Penrose effect is present ($\Delta K > 0$). Panel (g) shows the presence of negative current J_0 near the pump core, i.e., when $r/w \to 0$. The pump field has OAM $\ell = 1$ in all cases.

the current at $z = 4$ [see panel (g) of Fig. 1], which shows that J_0 is negative as expected when having superradiance. The reflection and transmission coefficients are also plotted [panel (h) of Fig. 1] and show an amplification of 20% at the end of the propagation.

More results are reported in Ref. 4 showing that if the full system is simulated, the evolution of the pump not only does not impede the process from happening, but rather favors it by allowing for less stringent phase-matching condition.

Summarizing, these simulations show consistently that to have superradiance one needs to satisfy the phase-matching condition, have trapping of the negative frequency modes, and have a negative flux (i.e., negative current) whenever $(n - \ell) > 0$. The effect disappears as soon as one of these conditions is not satisfied.

Recent experimental measurements have confirmed these numerical results,[25] demonstrating the feasibility of this effect in the laboratory. These results show an amplification of positive frequency modes and the trapping of the idler in the analog black hole ergoregion. Figure 2 reports the experimental currents in the same cases simulated above: the non-superradiant case with $n = -1$ and $q = 3$ [Fig. 2(a)] and the superradiance case with $n = 2$ and $q = 0$ [Fig. 2(a)].

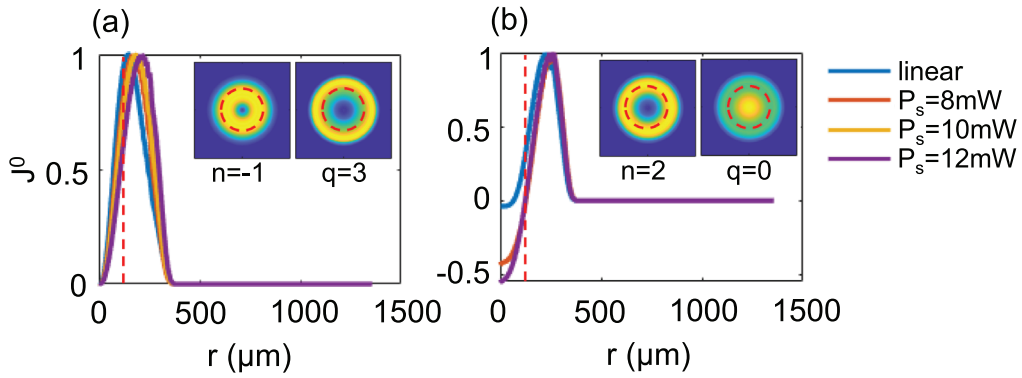

Fig. 2. Experimental results. Current $J_0(r)$ as a function of the radius r. The pump OAM is $\ell = 1$. (a) The signal has OAM $n = -1$ and idler OAM $q = 3$. Superradiance conditions are not met and the current is always positive. (b) $n = 2$ and $q = 0$. Superradiance occurs and the current J_0 is negative near the ergoregion indicated by the dashed red line ($r_e = 118\ \mu$m). Insets show the signal and idler intensity profiles $|E_{s,i}(r)|$ at the output of the nonlinear propagation in a solution of methanol and graphene. The idler is trapped in the pump vortex core in the superradiant cases (b). The different colors of the lines show the difference between linear and nonlinear propagation. When nonlinearity is excited, the superradiance effect can occur.

The pump vortex has OAM $\ell = 1$. The insets show the signal and idler transverse intensity profiles at the end of the nonlinear propagation and reports the trapping of the idler inside the ergoregion (dashed red line) when superradiance occurs. A maximum amplification of 5% is found.

E. Transient growth

In this section, we describe an approximate coupled-mode theory (CMT) that elucidates the gain mechanism that underpins the Penrose process in our nonlinear optical system. The approximation is motivated by the results shown in Figs. 1(a) and 1(e) where we see that the input signal undergoes what looks close to linear propagation with a focus around $z = 0$. To lowest order, we therefore approximate the signal beam transverse profile as proportional to the linearly evolving input Laguerre–Gaussian beam. Moreover, since the FWM process generates an idler field with a source that is proportional to the complex conjugate of the signal beam, we assume that the idler beam transverse profile is proportional to the complex conjugate of the same Laguerre–Gaussian beam.

To proceed, as above we write the signal beam as

$$\mathscr{E}_s(r,\theta,z) = c_s(z)U_n(r,z)e^{in\theta}e^{i\beta z}, \tag{44}$$

where the normalized radial mode function $U_n(r,z)$ obeys the free-space paraxial wave equation

$$\frac{\partial U_n}{\partial z} = \frac{i}{2k}\nabla_n^2 U_n. \tag{45}$$

This is a valid approximation if the signal beam is much narrower than the pump beam and does not overlap the pump core significantly: The pump beam then appears to have a homogeneous intensity profile as experienced by the signal beam. Upon propagation, the nonlinear interaction generates an idler with winding number $q = (2\ell - n)$, and we approximate the propagating idler field as

$$\mathscr{E}_i(r,\theta,z) = c_i(z)U_n^*(r,z)e^{iq\theta}e^{i\beta z}. \tag{46}$$

Then, substituting this form for the signal and idler fields into Eq. (5), using Eq. (45) for the radial mode function, and projecting separately with $U_n^*(r,z)e^{-in\theta}$ and $U_n(r,z)e^{-iq\theta}$, yields the equations for the signal and idler amplitudes as follows:

$$\begin{aligned}\frac{dc_s}{dz} &= i(2\Gamma_n - 1)\beta c_s + i\Gamma_n\beta c_i^*,\\ \frac{dc_i}{dz} &= \frac{i}{2k}\left[-2K_n^2 + \delta K_n^2\right]c_i + i(2\Gamma_n - 1)\beta c_i + i\Gamma_n\beta c_s^*,\end{aligned} \tag{47}$$

with the z-dependent projection factors

$$\Gamma_n(z) = \int_0^\infty dr\, r u_\ell^2(r)|U_n(r,z)|^2, \tag{48}$$

$$-K_n^2(z) = \int_0^\infty dr\, r U_n^*(r,z)\nabla_n^2 U_n(r,z), \tag{49}$$

$$\delta K_n^2(z) = (n^2 - q^2)\int_0^\infty dr\, r|U_n(r,z)|^2/r^2. \tag{50}$$

The above equations define the CMT and are solved along with the boundary conditions $c_s(z_i) = 1$ and $c_i(z_i) = 0$, with z_i the coordinate of the medium input. The last terms in both equations in Eq. (47) account for the nonlinear FWM interactions, and the other terms describe terms related to phase-matching of the process such as XPM and beam diffraction. The reflection and transmission coefficients may be calculated along the propagation direction using Eq. (41) as follows:

$$R(z) = (|c_s(z)|^2 - |c_i(z)|^2)\underbrace{\int_{r_e}^\infty |U_n(r,z)|^2 r dr}_{O(z)}, \tag{51}$$

and $T(z) = 1 - R(z)$. The overlap factor $O(z)$ involves a radial integral extending from the ergoradius r_e to infinity as this captures that portion of the propagating beam intensity profile that is reflected radially outside the ergosphere.

We have solved the CMT equations numerically for the parameters in Fig. 1 and the results for $(R-1)$ and T invariably look like those in plot (d) of Fig. 1, meaning that the CMT can only capture the case when the Zel'dovich–Meisner condition is not satisfied, and the Penrose process is absent, but not if it is satisfied. In particular, in Fig. 1(d) the reflectivity remains less than or equal to unity. This is readily understood from the CMT: First, one can prove that $(|c_s(z)|^2 - |c_i(z)|^2) = 1$ is a conserved quantity, so that the $R(z) = O(z)$. For a beam far removed on either side from the focus, we find $O(z) \to 1$, whereas $O(z) < 1$ around the focus as the Laguerre–Gaussian beam protrudes into the ergosphere. Thus, the shape of $R(z)$ versus z in Fig. 1(d) is essentially a measure of how much the incident signal LG beam protrudes into the ergoregion.

To elaborate further, if the phase-matching terms are neglected in Eq. (47) leaving only the FWM terms, the resulting two-state system comprised of the signal and idler can exhibit both amplification or loss: This is the limit of two-mode parametric amplification, which can lead to nonlinear instabilities.[59] In contrast, for the parameters appropriate to our proposed experiments the phase-matching terms detune the system so that the two-mode parametric amplification is inoperative, and what arises instead is an oscillatory exchange of power between the signal and idler: This is the so-called phase-conjugate coupling regime where the system dynamics is akin to a lossless system of two coupled oscillators described by a Hermitian Hamiltonian.[59]

As it is, the CMT does not describe the superadiant regime. The missing ingredient from the CMT is that it does not account for the energy that is transferred to the trapped idler wave alluded to in Sec. II A, and this can be accounted for by including a loss term $-\alpha(z)c_i/2$ on the right-hand side of the idler equation in (47): We treat the loss coefficient $\alpha(z)$ as a fit parameter that is applied only after the FWM interaction initiates in the vicinity of the signal beam focus. Physically, the introduction of the loss term in the idler Eq. (47) allows the transfer of idler energy into the trapped potential generated by the pump beam. This guiding/trapping potential stops the oscillatory exchange of energy between the signal and idler, favoring the signal amplification. Results from the CMT including idler absorption are shown in Fig. 3 corresponding to the full simulation in Fig. 1(h) with good qualitative agreement, both showing the Penrose process at the output with $(R-1) > 0$. The qualitative picture given by the CMT was found to be quite robust against variation in the fit parameters employed, giving confidence in the physics underlying extending the CMT to include idler absorption.

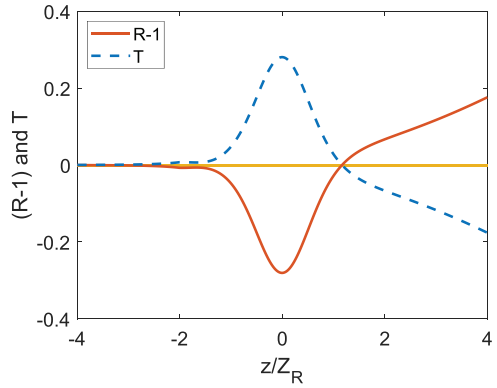

FIG. 3. Reflection $(R-1)$ and transmission T coefficients along the z axis. Losses start at $z/Z_R = -2$, where the interaction between the signal beam and the pump starts being phase-matched, with loss coefficient $\alpha = 2.6$.

These CMT results are relevant for a few reasons: First, they again highlight that excitation of the trapped idler mode is key to observing the Penrose process. Second, in order to see amplified reflection it is necessary to add idler absorption to the Hermitian two-state system (in the phase-conjugate regime) represented by the signal and idler.[60] The Penrose process may then be viewed as an example of the counter-intuitive phenomenon of transient growth in which non-Hermitian systems with non-normal modes can exhibit gain or amplification, at least transiently: Our two-mode system is rendered non-Hermitian by the addition of the absorption only to the idler mode. Finally, another view is that the addition of the losses changes the FWM interaction from the phase-conjugate to the two-mode parametric amplification regime, a manifestation of parity-time symmetry breaking that accompanies the Zel'dovich effect in nonlinear optics.[60] In this sense the CMT, although approximate, serves to deepen our understanding of the physics underlying the Penrose process.[2,61–66]

V. SUMMARY

Our goal in this Perspective has been to describe how a relatively modest nonlinear optics experimental setting can be used to elucidate the physics involved in the Penrose process. To this end, we have threaded together developments from four of our previous works that have culminated in our recent experiment. In the first step, we discussed how thermo-optic beam propagation may be viewed as a photon superfluid complete with a spectrum of Bogoliubov excitations, this perspective being key as it is these quasi-particles that participate in the Penrose process. Second, we discussed how rotating spacetime geometries can be realized by extending the photon superfluid picture and associated Bogoliubov analysis to allow for vortex fields that carry orbital angular momentum, thus providing a view that includes the notion of an ergoregion and Bogoliubov quasi-particles that can split apart. In the third step, we discussed an experimentally feasible geometry in which the Penrose process can be measured in more detail than before: Not only can the amplified reflection be measured, but the component that becomes trapped in the ergoregion can be measured, along with the generation of negative norm idler modes alluded to in our fourth work. In the final section, we provided a discussion of how the Penrose process may be viewed as arising from transient gain and parity-time-symmetry breaking, new views that arose from our studies.

Roger Penroses's work has motivated us to reach for tabletop experiments to explore gravitational phenomena that cannot be observed astrophysically at present. Indeed, recent reports have shown that these experiments are indeed possible and allow for example to observe for the first time the dynamics of both positive and negative norm modes.[25] We hope that this Perspective illustrates the utility of nonlinear optics as an analog-gravity system and motivates further exploration of the Penrose process and beyond.

ACKNOWLEDGMENTS

M.C.B. and D.F. acknowledge financial support from EPSRC (UK Grant No. EP/P006078/2) and the European Union's Horizon 2020 research and innovation program (Grant Agreement No. 820392). E.M.W. would like to thank Fergus Wright for insightful discussions regarding waves in rotating systems.

AUTHOR DECLARATIONS

Conflict of Interest

The authors have no conflicts to disclose.

DATA AVAILABILITY

Data sharing is not applicable to this article as no new data were created or analyzed in this study.

REFERENCES

[1]R. Penrose, Riv. Nuovo Cimento **1**, 252 (1969); Gen. Relativ. Gravitation **34**, 1141 (2002).
[2]R. Penrose and R. Floyd, Nat. Phys. Sci. **229**, 177 (1971).
[3]M. C. Braidotti, A. Vinante, G. Gasbarri, D. Faccio, and H. Ulbricht, Phys. Rev. Lett. **125**, 140801 (2020).
[4]M. C. Braidotti, D. Faccio, and E. M. Wright, Phys. Rev. Lett. **125**, 193902 (2020).
[5]A. Prain, C. Maitland, D. Faccio, and F. Marino, Phys. Rev. D **100**, 024037 (2019).
[6]F. Marino, M. Ciszak, and A. Ortolan, Phys. Rev. A **80**, 065802 (2009).
[7]F. Marino, Phys. Rev. A **78**, 063804 (2008).
[8]F. Belgiorno, S. L. Cacciatori, M. Clerici, V. Gorini, G. Ortenzi, L. Rizzi, E. Rubino, V. G. Sala, and D. Faccio, Phys. Rev. Lett. **105**, 203901 (2010).
[9]T. Roger, C. Maitland, K. Wilson, N. Westerberg, D. Vocke, E. M. Wright, and D. Faccio, Nat. Commun. **7**, 13492 (2016).
[10]D. Faccio, F. Belgiorno, S. Cacciatori, V. Gorini, S. Liberati, and U. Moschella, *Analogue Gravity Phenomenology: Horizons and from Theory to Experiment* (Springer, New York, 2013).
[11]D. Vocke, C. Maitland, A. Prain, K. E. Wilson, F. Biancalana, E. M. Wright, F. Marino, and D. Faccio, Optica **5**, 1099 (2018).
[12]C. Misner, Bull. Am. Phys. Soc. **17**, 472 (1972).
[13]T. Torres, S. Patrick, A. Coutant, M. Richartz, E. W. Tedford, and S. Weinfurtner, Nat. Phys. **13**, 833 (2017).
[14]W. G. Unruh, Phys. Rev. Lett. **46**, 1351 (1981).
[15]C. Barcelò, S. Liberati, and M. Visser, Living Rev. Relativ. **14**, 3 (2011).
[16]L. J. Garay, J. R. Anglin, J. I. Cirac, and P. Zoller, Phys. Rev. Lett. **85**, 4643 (2000).
[17]L. J. Garay, J. R. Anglin, J. I. Cirac, and P. Zoller, Phys. Rev. A **63**, 023611 (2001).
[18]R. Schützhold, G. Plunien, and G. Soff, Phys. Rev. Lett. **88**, 061101 (2002).
[19]S. Giovanazzi, C. Farrell, T. Kiss, and U. Leonhardt, Phys. Rev. A **70**, 063602 (2004).
[20]I. Zapata, M. Albert, R. Parentani, and F. Sols, New J. Phys. **13**, 063048 (2011).
[21]J. Steinhauer, Nat. Phys. **10**, 864 (2014).
[22]J. Steinhauer, Nat. Phys. **12**, 959 (2016).

[23]R. Brito, V. Cardoso, and P. Pani, *Superradiance* (Springer, 2015).
[24]D. D. Solnyshkov, C. Leblanc, S. V. Koniakhin, O. Bleu, and G. Malpuech, Phys. Rev. B **99**, 214511 (2019).
[25]M. Braidotti, R. Prizia, C. Maitland, F. Marino, A. Prain, I. Starshynov, N. Westerberg, E. Wright, and D. Faccio, Phys. Rev. Lett. **128**, 013901 (2022).
[26]D. Gerace and I. Carusotto, Phys. Rev. B **86**, 144505 (2012).
[27]M. Elazar, V. Fleurov, and S. Bar-Ad, Phys. Rev. A **86**, 063821 (2012).
[28]M. Ornigotti, S. Bar-Ad, A. Szameit, and V. Fleurov, "Analogue gravity by an optical vortex resonance enhancement of hawking radiation," arXiv:1704.07609 (2017).
[29]I. Carusotto, Proc. R. Soc. A **470**, 20140320 (2014).
[30]P.-E. Larré and I. Carusotto, Phys. Rev. A **92**, 043802 (2015).
[31]D. Vocke, T. Roger, F. Marino, E. M. Wright, I. Carusotto, M. Clerici, and D. Faccio, Optica **2**, 484 (2015).
[32]D. Vocke, K. Wilson, F. Marino, I. Carusotto, B. P. Anderson, P. Ohberg, and D. Faccio, Phys. Rev. A **94**, 013849 (2016).
[33]Q. Fontaine, T. Bienaime, S. Pigeon, E. Giacobino, A. Bramati, and Q. Glorieux, Phys. Rev. Lett. **121**, 183604 (2018).
[34]Y. B. Zel'dovich, Pis'ma Zh. Eksp. Teor. Fiz. **14**, 270 (1971) [JETP Lett. **14**, 180 (1971)].
[35]R. W. Boyd, *Nonlinear Optics* (Academic, 2002).
[36]U. Leonhardt, Philos. Trans. R. Soc., A **378**, 20190229 (2020).
[37]L. Diosi, Phys. Lett. A **120**, 377 (1987).
[38]R. Penrose, Gen. Relativ. Gravitation **28**, 581 (1996).
[39]R. Penrose, Found. Phys. **44**, 557 (2014).
[40]I. Carusotto, S. Fagnocchi, A. Recati, R. Balbinot, and A. Fabbri, New J. Phys. **10**, 103001 (2008).
[41]Q. Fontaine, P.-E. Larre, G. Lerario, T. Bienaime, S. Pigeon, D. Faccio, I. Carusotto, E. Giacobino, A. Bramati *et al.*, Phys. Rev. Res. **2**, 043297 (2020).
[42]C. Piekarski, W. Liu, J. Steinhauer, E. Giacobino, A. Bramati, and Q. Glorieux, Phys. Rev. Lett. **127**, 023401 (2021).
[43]M. Visser, Phys. Rev. Lett. **80**, 3436 (1998).
[44]L. P. Pitaevskii and S. Stringari, *Bose-Einstein Condensation* (Clarendon, Oxford, 2003).
[45]S. Weinfurtner, S. Liberati, and M. Visser, J. Phys. A **39**, 6807 (2006).
[46]S. Basak and P. Majumdar, Classical Quantum Gravity **20**, 3907 (2003).
[47]M. Visser and S. Weinfurtner, Classical Quantum Gravity **22**, 2493 (2005).
[48]R. Brito, V. Cardoso, and P. Pani, *Lecture Notes in Physics* (Springer, Heidelberg,, 2020), Vol. **971**, p. 107.
[49]K. S. Thorne, R. Price, and D. Macdonald, *Black Holes: The Membrane Paradigm* (Yale University, New Haven, CT, 1986).
[50]J. D. Bekenstein and M. Schiffer, Phys. Rev. D **58**, 064014 (1998).
[51]H. S. Ribner, J. Acoust. Soc. Am. **29**, 435 (1957).
[52]J. W. Miles, J. Acoust. Soc. Am. **29**, 226 (1957).
[53]D. J. Acheson, J. Fluid Mech. **77**, 433 (1976).
[54]S.-I. Takehiro and Y.-Y. Hayashi, J. Fluid Mech. **236**, 259 (1992).
[55]J. L. Friedman, Commun. Math. Phys. **63**, 243 (1978).
[56]N. Comins and B. F. Schutz, Proc. R. Soc. London, Ser. A **364**, 211 (1978).
[57]L. Giacomelli and I. Carusotto, Phys. Rev. Res. **2**, 033139 (2020).
[58]Y. Kivshar and G. Agrawal, *Optical Solitons* (Academic, Amsterdam, 2003).
[59]L. F. Buchmann, E. M. Wright, and P. Meystre, Phys. Rev. A **88**, 041801 (2013).
[60]D. Politzer, Am. J. Phys. **83**, 395 (2015).
[61]C. Gooding, S. Weinfurtner, and W. G. Unruh, Phys. Rev. A **101**, 063819 (2020).
[62]C. Gooding, Philos. Trans. R. Soc., Ser. A **378**, 2177 (2020).
[63]C. W. Misner, Phys. Rev. Lett. **28**, 994 (1972).
[64]W. H. Press and S. A. Teukolsky, Astrophys. J. **185**, 649 (1973).
[65]A. A. Starobinskii, Sov. Phys. JETP **37**(1), 28–32 (1973) [Zh. Eksp. Teor. Fiz. **64**, 48–57 (1973)], available at https://ui.adsabs.harvard.edu/#abs/1973JETP...37...28S/abstract.
[66]A. A. Starobinskil and S. M. Churilov, Zh. Eksp. Teor. Fiz. **65**, 3–11 (1973) [Sov. Phys. JETP **38**(1), 1–5 (1974)].